

Diffusion Model in Latent Space for Medical Image Segmentation Task

Ngoc Huynh Trinh*, Hai Toan Nguyen, Son Ba Luong, Quoc Long Tran[†]
Institute for Artificial Intelligence, University of Engineering and Technology,
Vietnam National University, Hanoi, Vietnam
Emails: {huynhntn, nguyenhaitoan, tqlong}@vnu.edu.vn,

[†]Corresponding author

Abstract: Medical image segmentation is essential for supporting clinical diagnosis and treatment planning. With growing imaging demands, artificial intelligence (AI) models are increasingly used to improve the accuracy and efficiency of this task while reducing the workload of radiologists. However, traditional approaches often produce a single segmentation mask per input image, limiting the ability to capture uncertainty in the segmentation process. Recent advancements in generative models for image generation present new opportunities to address these limitations by enabling the generation of multiple segmentation masks for each input image. Nevertheless, computational complexity and performance remain key challenges when operating directly in the image domain. In this work, we propose MedSegLatDiff, an effective framework for medical image segmentation that integrates a diffusion-based model (DM) with two variational autoencoders (VAEs) to decouple the segmentation process from perceptual data compression. Specifically, VAEs compress data into a low-dimensional latent space, reducing noise and accelerating learning, while the DM performs segmentation more efficiently within this latent representation. Furthermore, we replace the traditional Mean Squared Error (MSE) loss with a weighted Cross-Entropy (WCE) loss in the perceptual mask compression module, which enhances the reconstruction of segmentation masks during the encode–decode process, particularly for tiny nodules. Our designed framework emulates the collaborative segmentation approach of multiple clinicians, resulting in more robust and reliable performance compared to previous methods that model the segmentation patterns of individual practitioners. We evaluate our model on three datasets: ISIC-2018, CVC-Clinic, and LIDC-IDRI, demonstrating competitive performance while simultaneously providing the ability to generate confidence maps for deeper analysis by experts. Our results show that MedSegLatDiff achieves prominent segmentation performance while offering enhanced interpretability and consistency for clinical applications.

Keywords: diffusion model; variational autoencoder; medical image segmentation; conditional image generation.

I. INTRODUCTION

Medical image segmentation, which involves partitioning medical images into meaningful regions, plays a crucial role in clinical applications such as diagnosis, surgical planning, and image-guided procedures [3]. Accurate segmentation enables clinicians to better interpret images, facilitate comparisons, and monitor changes over time. However, manually labeling segmentation masks is time-consuming and labor-intensive, motivating the development of automated methods. While classical techniques

such as binary thresholding [6] and k-means clustering [4] have shown limited effectiveness [1], [5], [7], recent advances in AI have enabled the widespread adoption of machine learning (ML) and deep learning (DL) models, which achieve remarkable results [2].

Typically, these AI models are trained on pre-labeled datasets and can automatically segment new images. Most existing approaches adopt a one-to-one strategy, producing only a single segmented output per input image [9]–[12]. These methods basically learn a mapping function from each input image to a single segmentation mask, thereby replicating the behavior of an individual annotator. Recently, generative models, particularly diffusion models (DMs) [22], have led to substantial advances in image synthesis, often outperforming earlier approaches such as Generative Adversarial Networks (GANs) [21] and Variational Autoencoders (VAEs) [18], which remain among the most widely used methods in recent years. Beyond their success in natural image generation, these models open up new possibilities for medical image segmentation through a one-to-many paradigm. Unlike the previous one-to-one approach, diffusion-based models can generate multiple segmentation masks for a single input, capturing the model’s uncertainty in ambiguous medical data. Several recent studies have adopted this strategy and demonstrated superior performance and robustness compared to conventional methods [30]–[32], [38]. These results indicate that diffusion-based approaches not only enhance segmentation accuracy but also provide richer information to support clinical decision-making, particularly in challenging cases involving ambiguous or subtle anatomical structures. However, these models typically operate directly in the image space, where performance is limited because they are required to jointly perform image compression and region-of-interest analysis. Consequently, we identify opportunities to further improve model performance by conducting segmentation in a low-dimensional latent space.

In this paper, we propose MedSegLatDiff, a medical image segmentation framework that adopts a novel one-to-many paradigm based on DM. Our framework integrates two VAEs with a diffusion-based model and consists of two main stages. The first stage performs an encoder–decoder architecture to map the input image into a low-dimensional latent representation, while the second stage performs diffusion processes in the latent

space to generate a diverse set of segmentation masks for each input image. By conditioning the stochastic generation process of the diffusion model in the latent space, the model produces a set of segmentation masks corresponding to the input, whose variability captures the uncertainty typically exhibited by a group of clinicians. Thus, our model effectively simulates the segmentation consensus among multiple doctors and is well-suited for medical image segmentation tasks. Furthermore, the segmented results from the generated set of masks compete with those of previous models, while confidence maps derived from these outputs assist clinicians in making more thorough and reliable diagnoses. To the best of our knowledge, the main contributions of this paper are as follows:

- Training and incorporating VAEs to develop a conditional diffusion-based model in latent space, which reduces noise, compresses image into latent space, and improves both training and inference efficiency.
- Replacing Mean Squared Error (MSE) with weighted Cross-Entropy (WCE) in the VAE mask reconstruction stage improves the preservation of small structures, especially in cases involving tiny masks, thereby reducing the risk of neglect or misinterpretation as noise.
- Proposing MedSegLatDiff for medical image segmentation, which simulates the segmentation process of a group of clinicians by generating multiple outputs per input image to approximate their variance. Furthermore, confidence maps derived from these outputs assist experts in performing more thorough and reliable diagnoses.

The remainder of the paper is organized as follows. Section II reviews recent prominent studies on medical image segmentation, generative models, and autoencoder-based approaches. Section III describes the methods and techniques employed in the proposed model. Section IV presents experimental results on three datasets to demonstrate the model's effectiveness. Finally, Section V concludes the study and outlines potential directions for future research.

II. RELATED WORK

Medical Image Segmentation refers to the process of assigning a label to each pixel (or voxel) in a medical image to determine its class membership, thereby identifying regions of interest with diverse shapes. This problem has been extensively studied using various AI architectures, demonstrating superior performance compared to classical methods [2]. Early models followed a one-to-one paradigm, evolving from fully convolutional networks (FCNs) [8], which employ conventional CNN-based architectures, to encoder-decoder architectures with skip connections, such as U-Net [9] and U-Net++ [10], which extend skip connections to improve feature propagation. Traditional CNN-based models, including nnU-Net [11] and ResUNet [12], have demonstrated strong performance in medical image segmentation by effectively capturing hierarchical features and leveraging multi-scale contextual information. However, these methods are limited in modeling long-range dependencies, which are essential for

capturing global contextual information in complex medical images. To address this limitation, transformer-based architectures such as SegFormer [16], TransUNet [13], and SwinUNet [14] have been introduced to enable more comprehensive image analysis through deep transformer blocks at the cost of increased computational complexity and memory consumption. In addition, hybrid approaches that incorporate hypernetworks, such as HyperSeg [17], have been explored but remain complex and insufficiently mature. Overall, although these methods are still actively developing and show promising performance, they largely follow a one-to-one paradigm and are unable to explicitly model uncertainty in the segmentation process, which is crucial in medical applications.

Deep Generative Models were initially developed for image generation and synthesis, but their ability to learn underlying data distributions has recently drawn increasing attention in medical image segmentation and uncertainty modeling. Among them, Variational Autoencoders (VAEs) [18], which rely on probabilistic latent variable modeling, and Generative Adversarial Networks (GANs) [21], which learn through adversarial training, laid the foundation for modern deep generative modeling. More recently, diffusion models (DMs) [22], which generate images by gradually adding and then removing noise through a Markov chain process, have achieved state-of-the-art performance across various tasks, often matching or surpassing advanced GAN techniques [25]. By incorporating conditioning into the generation process, several diffusion-based models have been successfully applied to various domains, including medical image segmentation. For example, EnsembleDiff [30] conditions the diffusion process by concatenating medical images with their noisy counterparts during denoising, whereas SegDiff [31] adds (rather than concatenates) the input image via element-wise addition after passing it through a convolutional encoder. Notably, MedSegDiff [32] and MedSegDiff-v2 [33] further introduce a Feature Frequency Parser to mitigate high-frequency noise and employ a Spectrum-Space Transformer to enhance semantic feature interaction. Other conditioning approaches include guided diffusion for universal anatomical segmentation [36] and prompt-guided variants such as ProGiDiff [37], which adapt pre-trained latent diffusion models for flexible conditioning. In parallel, applications of diffusion models have continued to evolve to alleviate the computational burden. Two major directions have emerged: performing the diffusion process in a low-dimensional latent space, as exemplified by Stable Diffusion [27], and accelerating the inference process through improved sampling strategies such as DDIM [24] and PLMS [43]. The former has proven effective for a wide range of tasks, including image inpainting, class-conditional synthesis, text-to-image generation, unconditional image generation, and super-resolution [27]–[29]. The latter direction has been widely explored in medical image segmentation. For instance, LSegDiff [34] proposes a fast latent diffusion model evaluated on polyp and skin lesion segmentation tasks, while LDSeg [35] introduces an end-to-end conditional latent diffusion framework that leverages low-dimensional shape manifolds for multi-modal segmentation, achieving

faster sampling and reduced memory consumption than pixel-space diffusion methods.

While these prior works demonstrate the promise of latent diffusion in improving efficiency and accuracy for medical image segmentation, most rely on standard VAEs or pixel-space conditioning and do not explicitly address challenges such as tiny or sparse target structures (e.g., small nodules) through specialized loss designs, such as weighted reconstruction. Motivated by these observations, we propose MedSegLatDiff, a latent diffusion framework that integrates VQ-VAE [19], [20] for discrete and stable compression of both images and segmentation masks. In particular, a WCE reconstruction loss is incorporated into the mask VQ-VAE to replace the conventional MSE loss, thereby improving the preservation of small and sparse structures. Furthermore, stochastic sampling in the latent space enables a one-to-many paradigm that generates multiple plausible segmentation masks for a given input, capturing variability comparable to that observed among groups of clinicians. As a result, MedSegLatDiff is particularly well suited for ambiguous and challenging medical data, where uncertainty modeling can provide valuable support for clinical decision-making.

III. METHOD

In this section, we introduce our proposed MedSegLatDiff framework, which integrates a conditional diffusion-based model with two VAEs for medical image segmentation. We begin with an overview of conditional diffusion models for image-space segmentation, followed by a description of the VAEs used to encode and decode medical images and segmentation masks. We then present our latent diffusion model with conditioning mechanisms operating in the latent space for this task.

A. Segmentation in image space

Medical image segmentation is formulated under the assumption that a labeled dataset is available, where each image is paired with a ground-truth segmentation mask. Formally, we consider a medical imaging dataset:

$$\mathcal{D} = \{(X^{(i)}, S^{(i)})\}_{i=1}^N, \quad (1)$$

where $X^{(i)} \in \mathbb{R}^{H \times W \times C}$ denotes the i -th medical image, $S^{(i)} \in \{0, 1\}^{H \times W}$ is its corresponding segmentation mask, and N is the total number of image-mask pairs in this dataset \mathcal{D} . The main idea when applying DM for segmentation task is to gradually add noise $\epsilon \sim \mathcal{N}(0, I)$ to a mask S through a forward process and progressively remove noise from the noisy image via a reverse process. The forward process starts with the original image S_0 sampled from the mask distribution $p_{\text{mask}}(S)$ and is defined as:

$$q(S_t | S_{t-1}) = \mathcal{N}(S_t; \sqrt{\alpha_t} S_{t-1}, (1 - \alpha_t)I), \quad (2)$$

S_t denotes the latent variable at step t in the Markov chain, and α_t is the noise scheduler controlling the noise variance at each step. Over the course of T steps, the forward process generates progressively noisier images (S_1, S_2, \dots, S_T) , with $S_T \sim \mathcal{N}(0, I)$ representing the noisiest image. Given S_0 , a desirable property of this process [22] is that the marginal distribution of S_t can

be obtained by analytically marginalizing out the intermediate latent variables:

$$q(S_t | S_0) = \mathcal{N}(S_t; \sqrt{\gamma_t} S_0, (1 - \gamma_t)I). \quad (3)$$

where $\gamma_t = \prod_{i=1}^t \alpha_i$. This forward process generates noisy image pairs that serve as training data for a denoising model $\epsilon_\theta(S_t, t)$. The model takes the noisy image S_t as input and the added noise ϵ at step t as the target. In its simplest form, the model is trained using the MSE loss:

$$\mathcal{L}_{\text{simple}} = \mathbb{E}_{\epsilon \sim \mathcal{N}(0, I), t} \|\epsilon - \epsilon_\theta(S_t, t)\|_2^2, \quad (4)$$

and the noise estimator $\epsilon_\theta(S_t, t)$ is implemented using a U-Net architecture [22].

During inference, the reverse distribution $q(S_{t-1} | S_t, S_0)$ is approximated using the trained denoising model. Starting from pure Gaussian noise $S_T \sim \mathcal{N}(0, I)$, the noise is iteratively removed at each timestep to recover S_{t-1} . This procedure is referred to as the reverse diffusion process and is performed as follows:

$$S_{t-1} = \frac{1}{\sqrt{\alpha_t}} \left(S_t - \frac{\sqrt{1 - \alpha_t}}{\sqrt{1 - \gamma_t}} \epsilon_\theta(S_t, t) \right) + \gamma_t \epsilon', \quad (5)$$

where $\epsilon' \sim \mathcal{N}(0, I)$ introduces stochasticity into the reverse process, and $t = T, \dots, 1$ denotes the reverse diffusion steps. By repeating the reverse process for T timesteps, the model generates a segmentation mask S_0 as an approximate sample from the underlying distribution of segmentation masks. Moreover, repeated stochastic sampling enables the generation of multiple plausible segmentation masks, effectively approximating this distribution.

However, the formulation described above only generates unconditional random masks and cannot perform segmentation conditioned on a given input image. To address this limitation, following prior studies, we incorporate conditioning into the generation process, enabling the model to generate a corresponding segmentation mask for a given input image. Specifically, given a medical image X and its corresponding segmentation mask S , we adapt the model for the segmentation task by appending X as an additional input channel to incorporate anatomical information into each noisy mask S_t . As a result, the noisy mask and the input image are concatenated channel-wise to obtain

$$S_t^{\text{cond}} := S_t \oplus X, \quad (6)$$

where \oplus denotes channel-wise concatenation. The resulting conditioned representation is then fed into the modified denoising model $\epsilon(S_t^{\text{cond}}, t)$. This concatenation guides the denoising process, ensuring that the model generates new masks corresponding to the input image X . During the forward process, noise is added only to the ground truth segmentation S , while X remains unchanged to preserve anatomical guidance. Since the sampling process is stochastic, the diffusion model generates multiple segmentation masks S_0 for each input image X . When trained with a single segmentation mask per image, the model implicitly produces an ensemble of masks, effectively emulating the consensus-driven segmentation process of a group of doctors and potentially improving overall performance.

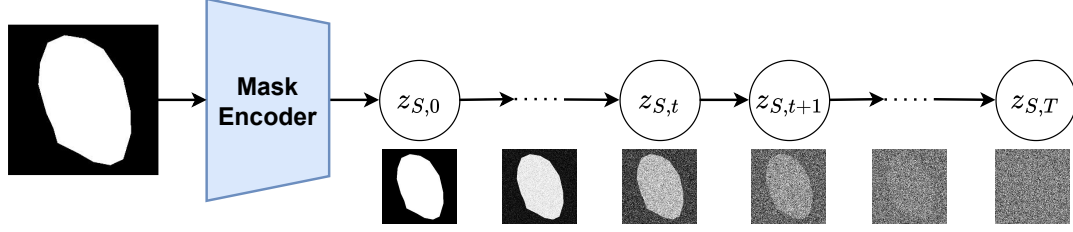


Figure 1: Illustration of the forward diffusion process in latent space, in which Gaussian noise is progressively added to the encoded segmentation mask across diffusion timesteps.

B. Image and Mask in latent space

The VAE [18] is a neural network that maps each image from the data distribution to a latent code in a lower-dimensional latent space. It consists of an encoder $\mathcal{E}(\cdot)$ and a decoder $\mathcal{D}(\cdot)$. The encoder maps an image $X \in \mathbb{R}^{H \times W \times C}$ to a latent representation $z = \mathcal{E}(X)$, while the decoder reconstructs the image as $X' = \mathcal{D}(z) = \mathcal{D}(\mathcal{E}(X))$, where $z \in \mathbb{R}^{h \times w \times c}$ lies in a lower-dimensional latent space. The encoder downsamples the image by a factor $f = \frac{H}{h} = \frac{W}{w}$, and in our study, we investigate different downsampling factors of the form $f = 2^m$ with $m \in \mathbb{N}$. For our segmentation task, both the medical image X and the corresponding segmentation mask S must be transformed into the same low-dimensional latent space. To achieve this, we employ two separate autoencoders trained independently for images and masks. In particular, we adopt the Vector Quantized Variational Autoencoder (VQ-VAE) [19], [20], whose discrete latent space has demonstrated strong generative performance in recent models such as Stable Diffusion [27]. VQ-VAE is particularly suitable for our setting because: (i) its discrete codebook provides a stable, expressive latent representation; (ii) the quantized latent space is naturally compatible with diffusion models, as demonstrated in Stable Diffusion [27]; and (iii) the stop-gradient mechanism stabilizes training and preserves the piecewise-constant structure characteristic of segmentation masks.

First, we employ a VQ-VAE to encode the input image into a latent space and guide the generation process, ensuring that the predicted mask corresponds to the input image rather than being arbitrary. It consists of an encoder $\mathcal{E}_X(\cdot)$ that maps the input image X to a latent representation z_X , and a decoder $\mathcal{D}_X(\cdot)$ that reconstructs the image. In addition, a quantization module $Q_{z_X}(\cdot)$ is designed to discretize the continuous latent representation z_X into $\bar{z}_X = Q_{\mathcal{V}_X}(z_X)$ using a codebook $\mathcal{V}_X = \{v_X^{(k)}\}_{k=1}^K$. Specifically, each d -dimensional vector in z_X is replaced by its nearest codebook entry, and the codebook is jointly learned during training. The optimization objective combines three synergistic terms: a reconstruction loss to ensure high-fidelity reconstructions

$$\mathcal{L}_{\text{rec}} = \|X - \mathcal{D}_X(\bar{z}_X)\|_2^2, \quad (7)$$

a codebook loss to align encoder outputs with the nearest embeddings

$$\mathcal{L}_{\text{codebook}} = \|\text{sg}(z_X) - \bar{z}_X\|_2^2, \quad (8)$$

and a commitment loss to prevent the encoder outputs from fluctuating excessively

$$\mathcal{L}_{\text{commit}} = \beta \|z_X - \text{sg}(\bar{z}_X)\|_2^2. \quad (9)$$

Here, $\text{sg}[\cdot]$ denotes the stop-gradient operator, which prevents gradients from flowing into its argument during backpropagation, ensuring that the encoder and the codebook are updated separately. The full objective is then given by

$$\mathcal{L}_{\text{VQ-VAE}} = \mathcal{L}_{\text{rec}} + \mathcal{L}_{\text{codebook}} + \mathcal{L}_{\text{commit}}. \quad (10)$$

Secondly, we design another VQ-VAE for the segmentation mask to enable the diffusion-based model to learn the mask distribution in the latent space more efficiently and effectively. It is structured similarly to the image VQ-VAE and consists of an encoder $\mathcal{E}_S(\cdot)$, a decoder $\mathcal{D}_S(\cdot)$, and a quantization module $Q_{\mathcal{V}_S}(\cdot)$, which discretizes the latent representation using a codebook $\mathcal{V}_S = \{v_S^{(k)}\}_{k=1}^K$. The key difference lies in our modified loss function, which focuses on the segmented region, with particular emphasis on tiny nodules in the LIDC-IDRI dataset. Instead of using MSE for reconstruction, we adopt WCE to better capture the characteristics of small and sparse lesion regions. The modified reconstruction loss assigns larger weights to pixels within the segmentation mask, enabling the model to focus on these regions and reconstruct the mask more accurately, while all other loss components remain unchanged. This design prevents the perceptual compression model from ignoring tiny nodules, which might otherwise be mistakenly treated as noise.

C. Segmentation in latent space

Once the two pre-trained VQ-VAE models, one for medical images and the other for the corresponding segmentation masks, are prepared as described in Part III-B, we perform the diffusion processes in the latent domain. For each pair of medical image $X \in \mathbb{R}^{H \times W \times C}$ and segmentation mask $S \in \mathbb{R}^{H \times W}$, the corresponding latent representations are obtained as \bar{z}_X and \bar{z}_S . Using the latent representations, the diffusion model performs the forward diffusion process on each latent mask $z_{S,0} = \bar{z}_S$, as illustrated in Fig. 1. This process follows the diffusion mechanism described in Eqs. 2 and 3, which generate noisy labels for the data and train the denoising model.

Similarly, to generate segmentation masks for a medical image X that are consistent with the input rather than arbitrary, the denoising model incorporates additional

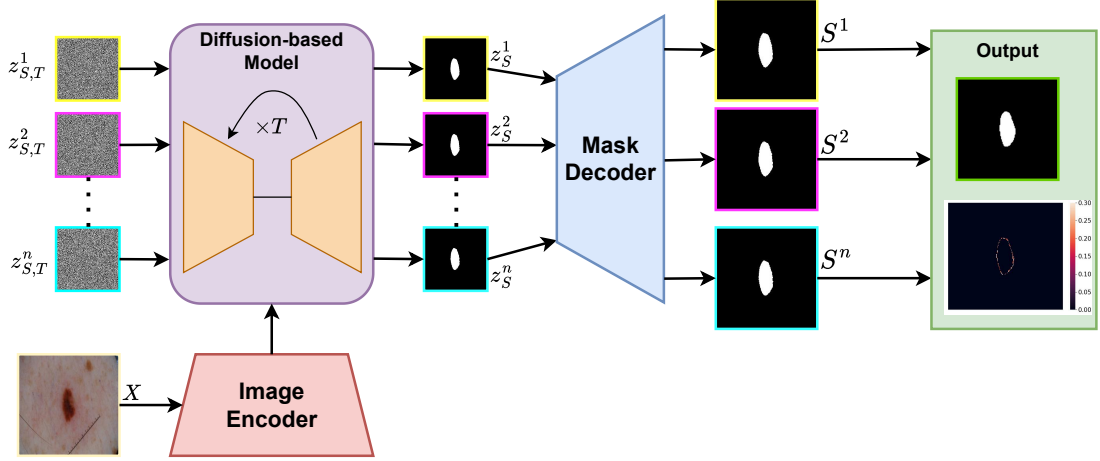


Figure 2: Overview of segmentation pipeline: multiple segmentation masks are generated from random noise in the latent space for a given medical image, followed by decoding, consensus fusion, and confidence map estimation.

conditions derived from the image. These conditions guide the noise removal process and the generation of the corresponding segmentation mask. Specifically, the denoising model takes as input a combination of the noisy mask $z_{S,t}$ and the latent image representation \bar{z}_X as a conditioning signal, using a concatenation operator in the latent space:

$$z_{S,t}^{\text{cond}} = z_{S,t} \oplus \bar{z}_X \quad (11)$$

The denoising model $\epsilon_\theta(z_{S,t}^{\text{cond}}, t)$ is then trained for the reverse diffusion process. Accordingly, the reverse process in Eq. 5 is modified to incorporate the conditioning as follows:

$$S_{t-1} = \frac{1}{\sqrt{\alpha_t}} \left(S_t - \frac{\sqrt{1-\alpha_t}}{\sqrt{1-\gamma_t}} \epsilon_\theta(z_{S,t}^{\text{cond}}, t) \right) + \gamma_t z \quad (12)$$

Thus, during the inference process, for each latent medical image \bar{z}_X , a set of n segmentation masks in the latent space, $\mathcal{Z}_{S,0} = \{z_S^1, z_S^2, \dots, z_S^n\}$, is generated from a corresponding set of Gaussian noises, $\mathcal{Z}_{S,T} = \{z_{S,T}^1, \dots, z_{S,T}^n\}$. The final step is to map the latent masks back to the original image space using the segmentation mask decoder:

$$S^i = \mathcal{D}_S(z_S^i), \quad (13)$$

where $i = 1, 2, \dots, n$. The final output of the model is the set of segmentation masks $\mathcal{S} = \{S^1, S^2, \dots, S^n\}$, which can be used to compute a confidence map and generate an implicit ensemble segmentation map. The final consistent result is obtained by averaging the outputs in the set to compute a confidence map, which is then thresholded at 0.5 to produce the final binary segmentation mask. The entire segmentation process is illustrated in Fig. 2. It can fully mimic the segmentation performed by a group of n doctors, which helps to improve the model's performance.

IV. EXPERIMENTS

A. Datasets

We conducted experiments on three publicly available datasets. The first dataset, ISIC-2018 [39], was released for the ISIC Skin Image Analysis Workshop and Challenge 2018 (Task 1), which focuses on automated binary segmentation of skin lesion regions in dermoscopic images. The dataset was obtained from the official ISIC Challenge website¹ and consists of dermoscopic images collected from multiple clinical centers. The second dataset, CVC-Clinic [40], comprises frames extracted from endoscopy videos and is widely used for polyp segmentation in medical images. It is publicly available on Kaggle². The third dataset, LIDC-IDRI [41], consists of thoracic CT scans with lesion annotations provided by four experienced radiologists. Only slices containing nodules were extracted, and the four radiologist-annotated masks were averaged to form a single consensus mask used as the ground-truth target. Unlike the first two datasets, LIDC-IDRI was split on a patient-wise basis into training, validation, and testing sets with an 8:1:1 ratio. For ISIC-2018 and CVC-Clinic, the default dataset-provided splits were used.

B. Implementation Details

We employ a VQ-VAE to compress both medical images and segmentation masks, followed by a diffusion-based model operating in the latent space for segmentation. The VQ-VAE adopts an autoencoder architecture with three downsampling and upsampling levels, while the diffusion model is implemented as a U-Net with a matching three-level configuration. Both networks use 64 base channels with channel multipliers [1, 2, 4]. For mask

¹<https://challenge.isic-archive.com/data/#2018>

²<https://www.kaggle.com/datasets/balraj98/cvcclinicdb>

compression, a Weighted Cross-Entropy (WCE) loss is applied, with a positive-class weight of 5 for ISIC-2018 and CVC-Clinic, and 50 for LIDC-IDRI to account for the extremely small target regions. The diffusion model follows the training setup described in [22], using 1000 diffusion timesteps. To condition the diffusion process, the encoded input image is directly concatenated with the noisy latent representation, serving as guidance during both training and inference. Images from ISIC-2018 and CVC-Clinic are resized to 256×256 pixels, while LIDC-IDRI slices are resized to 128×128 . Training is performed using the AdamW optimizer [42], with batch sizes of 32 for ISIC-2018 and CVC-Clinic and 64 for LIDC-IDRI. The initial learning rate is set to 1×10^{-4} . During inference, five stochastic samples are generated per input and aggregated by averaging to obtain a confidence map, which is thresholded at 0.5 to produce the final segmentation. For fair comparison, diffusion-based baselines are reproduced under identical settings. Performance is evaluated using PSNR [45] and SSIM [44] for the reconstruction task, and the Dice coefficient and Intersection over Union (IoU) for the segmentation task. All experiments are implemented in PyTorch and conducted on four Tesla V100 GPUs with 16 GB memory each.

C. Results

We first trained two separate VQ-VAE models for images and segmentation masks to enable latent-space mapping, and then trained a conditional diffusion model on the learned latent distributions. Table I reports the reconstruction performance of the VQ-VAE models

Table I: Performance of VQ-VAE for perceptual data compression.

Dataset	Input (loss)	Dice	IoU	SSIM	PSNR
ISIC-2018	Mask (MSE)	98.0	96.5	0.975	38.0
	Mask (WCE)	98.4	96.9	0.98	38.4
	Image (MSE)	-	-	0.94	34.2
CVC-Clinic	Mask (MSE)	99.0	98.9	0.976	38.0
	Mask (WCE)	99.5	99.0	0.98	38.7
	Image (MSE)	-	-	0.94	34.5
LIDC-IDRI	Mask (MSE)	88.0	83.1	0.92	35.2
	Mask (WCE)	94.4	89.4	0.99	41.7
	Image (MSE)	-	-	0.89	33.2

For image reconstruction, we employed the mean squared error (MSE) loss, achieving high reconstruction quality with SSIM of 0.94 and PSNR of approximately 34 on the ISIC-2018 and CVC-Clinic datasets, while lower performance was observed on the more challenging LIDC-IDRI dataset (SSIM 0.89, PSNR 33.2). For mask compression, using MSE loss resulted in strong segmentation fidelity, with Dice scores exceeding 98% and IoU scores above 96% on ISIC-2018 and CVC-Clinic. However, the presence of small and fine-grained structures in LIDC-IDRI led to reduced performance, with a Dice score of 88.0%. When switching to the WCE loss, performance improvements on the ISIC-2018 and CVC-Clinic datasets are marginal, as their segmentation masks typically cover relatively large regions. In contrast, the

LIDC-IDRI dataset shows substantial improvements, with Dice increasing by 6.4 points to 94.4, IoU improving by 6.3 points to 89.4, SSIM increasing by 0.07, and PSNR improving by 6.5 dB. Overall, only modest gains are observed on datasets with larger mask regions, while WCE proves particularly beneficial for datasets containing small and sparse structures. These results validate VQ-VAE’s effectiveness for latent-space compression of medical data, especially with WCE for sparse/tiny masks.

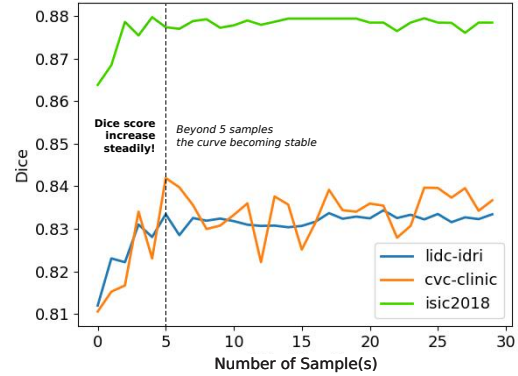


Figure 3: Dice scores versus the number of samples (ensemble size)

For the segmentation task, qualitative results of our model are first presented in Fig. 4. Five stochastic samples are generated for each input image and averaged to produce a confidence map, which is then thresholded at 0.5 to obtain the final segmentation mask. Results across all three datasets demonstrate that the generated masks closely match the ground-truth annotations, including the small target regions in the LIDC-IDRI dataset. Variations among sampled masks are mainly observed along object boundaries, which can be attributed to inherent ambiguities in medical images. By generating multiple segmentation masks, the proposed model produces a confident consensus prediction while explicitly capturing uncertainty through the confidence map. This uncertainty-aware output enhances the interpretability of the model and provides clinicians with additional insights for more informed analysis. Furthermore, we present the Dice score as a function of the number of samples in Fig. 3 to justify our choice of using five samples during inference. The segmentation performance improves steadily as the number of samples increases from 1 to 5, with Dice scores on ISIC-2018 rising from 0.865 to 0.880, on CVC-Clinic from 0.810 to 0.845, and on LIDC-IDRI from lower values to 0.834, indicating improved consensus as more stochastic samples are aggregated. Beyond five samples, performance gains gradually plateau (up to 30 samples), while computational cost continues to increase. Therefore, we adopt five samples as an effective trade-off between segmentation accuracy and inference efficiency.

Moreover, quantitative comparisons between our method and existing approaches are reported in Tables II and III. Table II shows that MedSegLatDiff achieves

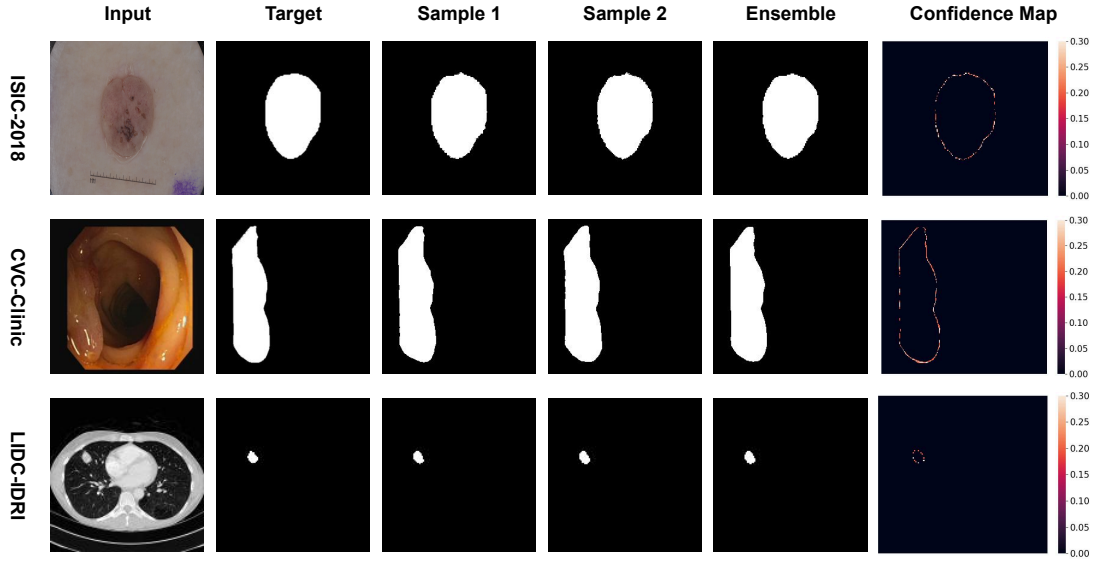


Figure 4: Visualization of multiple segmentation masks. The first two columns show the input image and the ground-truth mask, followed by two mask samples, their averaged output, and the resulting confidence map.

Table II: Comparison of MedSegLatDiff with previous one-to-one segmentation models.

Model	ISIC-2018		CVC-Clinic		LIDC-IDRI	
	Dice	IoU	Dice	IoU	Dice	IoU
UNet [9]	85.6	78.5	82.3	72.5	81.0	70.0
UNet++ [10]	81.0	72.9	79.4	70.9	79.9	68.9
ResUNet [12]	87.1	78.2	81.5	71.6	82.1	70.6
nnUNet [11]	87.5	79.5	81.3	71.3	82.8	71.0
MedSegLatDiff	88.0	80.5	84.5	73.1	83.4	71.8

competitive performance compared with one-to-one baselines. In particular, MedSegLatDiff obtains the highest Dice scores (88.0 / 84.5 / 83.4) and IoU (80.5 / 73.1 / 71.8) across all datasets, with consistent improvements ranging from 0.5 to 2.2 in Dice and from 0.5 to 0.8 in IoU compared to the best-performing competing methods. These results indicate the advantage of the proposed one-to-many modeling paradigm over conventional one-to-one approaches, highlighting its suitability for medical image segmentation tasks where ambiguity and inter-observer variability are inherent. In parallel, comparisons with one-to-many diffusion-based baselines are reported in Table III. MedSegLatDiff demonstrates competitive performance against other diffusion-based methods. Specifically, while it achieves comparable IoU and slightly lower Dice than MedSegDiff on ISIC-2018, it clearly excels on CVC-Clinic, improving Dice by 0.5 and IoU by 0.6. On the more challenging LIDC-IDRI dataset, where tiny and sparse masks pose greater difficulties, MedSegLatDiff further improves Dice by 0.9 and IoU by 0.7, highlighting its robustness in handling small target structures. Overall, these results demonstrate the effectiveness of latent-

space diffusion with VQ-VAE compression and WCE in achieving robust and uncertainty-aware medical image segmentation.

Table III: Comparison of MedSegLatDiff with recent one-to-many segmentation models.

Model	ISIC-2018		CVC-Clinic		LIDC-IDRI	
	Dice	IoU	Dice	IoU	Dice	IoU
EnsembleDiff [30]	86.6	79.5	83.5	71.9	81.7	70.5
SegDiff [31]	85.3	78.7	82.1	70.1	81.0	70.0
MedSegDiff [32]	88.1	80.5	84.0	72.5	82.5	71.1
MedSegLatDiff	88.0	80.5	84.5	73.1	83.4	71.8

Limitation: Despite the promising results, our method still has several limitations. In the current study, we only integrate VQ-VAEs to enable latent-space segmentation and have not yet systematically investigated the invariance properties of different VAE variants for comparison. In addition, although our experiments demonstrate that WCE is more effective than MSE for mask compression, further exploration of loss functions specifically designed for tiny or sparse object segmentation, such as Focal Loss or Dice-based losses, is necessary. These aspects constitute important directions for future work and will be explored in our subsequent studies to further improve segmentation robustness and uncertainty modeling.

V. CONCLUSION

In this paper, we propose MedSegLatDiff, a conditional diffusion framework that operates in a compressed latent space using VQ-VAE for efficient medical image segmentation. By employing two separate VQ-VAE modules for images and segmentation masks, our method achieves

effective perceptual compression while preserving critical structural details. Moreover, replacing the conventional MSE loss with a Weighted Cross-Entropy (WCE) loss for mask reconstruction substantially improves reconstruction quality, particularly for tiny and sparse structures such as nodules in the LIDC-IDRI dataset.

Our experiments demonstrate that generating five stochastic samples strikes a robust balance between computational cost and segmentation performance, producing stable ensemble predictions and reliable confidence maps. MedSegLatDiff consistently outperforms traditional one-to-one segmentation models and achieves competitive or superior performance compared to recent one-to-many diffusion-based approaches across ISIC-2018, CVC-Clinic, and LIDC-IDRI. The latent-space design effectively suppresses noise and allows the diffusion model to focus on the segmentation process, while the one-to-many paradigm captures segmentation uncertainty by mimicking inter-expert variability, thereby providing valuable support for clinical decision-making.

For future work, we plan to investigate advanced conditioning strategies, such as classifier guidance [25], classifier-free guidance [26], and flow-based generative modeling, to further enhance output stability, calibration, and uncertainty quantification.

ACKNOWLEDGMENT

The computing resources used in this research were sponsored by Intelligent Integration Co., Ltd. (INT2), Vietnam.

REFERENCES

- [1] K. K. D. Ramesh, G. K. Kumar, K. Swapna, D. Datta, and S. S. Rajest, "A review of medical image segmentation algorithms," *EAI Endorsed Trans. Pervasive Health Technol.*, vol. 7, no. 27, 2021.
- [2] G. Litjens et al., "A survey on deep learning in medical image analysis," *Med. Image Anal.*, vol. 42, pp. 60–88, 2017.
- [3] D. L. Pham, C. Xu, and J. L. Prince, "Current methods in medical image segmentation," *Annu. Rev. Biomed. Eng.*, vol. 2, no. 1, pp. 315–337, 2000.
- [4] H. P. Ng et al., "Medical image segmentation using k-means clustering and improved watershed algorithm," in *IEEE Sw. Symp. Image Anal. Interpret.*, 2006, pp. 61–65.
- [5] N. S. Hassan et al., "Medical images breast cancer segmentation based on K-means clustering algorithm: a review," *Asian J. Res. Comput. Sci.*, vol. 9, no. 1, pp. 23–38, 2021.
- [6] N. Senthilkumaran and S. Vaithegi, "Image segmentation by using thresholding techniques for medical images," *Comput. Sci. Eng. Int. J.*, vol. 6, no. 1, pp. 1–13, 2016.
- [7] S. Jardim, J. António, and C. Mora, "Image thresholding approaches for medical image segmentation-short literature review," *Procedia Comput. Sci.*, vol. 219, pp. 1485–1492, 2023.
- [8] J. Long, E. Shelhamer, and T. Darrell, "Fully convolutional networks for semantic segmentation," in *Proc. IEEE Conf. Comput. Vis. Pattern Recognit. (CVPR)*, 2015, pp. 3431–3440.
- [9] O. Ronneberger, P. Fischer, and T. Brox, "U-net: Convolutional networks for biomedical image segmentation," in *MICCAI*, 2015, pp. 234–241.
- [10] Z. Zhou et al., "Unet++: A nested u-net architecture for medical image segmentation," in *DLMA*, 2018, pp. 3–11.
- [11] F. Isensee et al., "nnU-Net: a self-configuring method for deep learning-based biomedical image segmentation," *Nature Methods*, vol. 18, no. 2, pp. 203–211, 2021.
- [12] F. I. Diakogiannis et al., "ResUNet-a: A deep learning framework for semantic segmentation of remotely sensed data," *ISPRS J. Photogramm. Remote Sens.*, vol. 162, pp. 94–114, 2020.
- [13] J. Chen et al., "Transunet: Transformers make strong encoders for medical image segmentation," *arXiv preprint arXiv:2102.04306*, 2021.
- [14] H. Cao et al., "Swin-unet: Unet-like pure transformer for medical image segmentation," in *ECCV*, 2022, pp. 205–218.
- [15] A. Hatamizadeh et al., "Unetr: Transformers for 3d medical image segmentation," in *Proc. IEEE/CVF WACV*, 2022, pp. 574–584.
- [16] E. Xie et al., "SegFormer: Simple and efficient design for semantic segmentation with transformers," *Adv. Neural Inf. Process. Syst.*, vol. 34, pp. 12077–12090, 2021.
- [17] Y. Nirkin, L. Wolf, and T. Hassner, "Hyperseg: Patchwise hypernetwork for real-time semantic segmentation," in *Proc. IEEE/CVF CVPR*, 2021, pp. 4061–4070.
- [18] D. P. Kingma and M. Welling, "Auto-encoding variational bayes," *arXiv preprint arXiv:1312.6114*, 2013.
- [19] A. Razavi, A. Van den Oord, and O. Vinyals, "Generating diverse high-fidelity images with vq-vae-2," *Adv. Neural Inf. Process. Syst.*, vol. 32, 2019.
- [20] J. Peng, D. Liu, S. Xu, and H. Li, "Generating diverse structure for image inpainting with hierarchical VQ-VAE," in *Proc. IEEE/CVF CVPR*, 2021, pp. 10775–10784.
- [21] I. Goodfellow et al., "Generative adversarial networks," *Commun. ACM*, vol. 63, no. 11, pp. 139–144, 2020.
- [22] J. Ho, A. Jain, and P. Abbeel, "Denosing diffusion probabilistic models," *Adv. Neural Inf. Process. Syst.*, vol. 33, pp. 6840–6851, 2020.
- [23] A. Q. Nichol and P. Dhariwal, "Improved denosing diffusion probabilistic models," in *ICML*, 2021, pp. 8162–8171.
- [24] J. Song, C. Meng, and S. Ermon, "Denosing diffusion implicit models," *arXiv preprint arXiv:2010.02502*, 2020.
- [25] P. Dhariwal and A. Nichol, "Diffusion models beat gans on image synthesis," *Adv. Neural Inf. Process. Syst.*, vol. 34, pp. 8780–8794, 2021.
- [26] J. Ho and T. Salimans, "Classifier-free diffusion guidance," *arXiv preprint arXiv:2207.12598*, 2022.

- [27] R. Rombach et al., "High-resolution image synthesis with latent diffusion models," in *Proc. IEEE/CVF CVPR*, 2022, pp. 10684–10695.
- [28] W. H. L. Pinaya et al., "Brain imaging generation with latent diffusion models," in *MICCAI Workshop Deep Generative Models*, 2022, pp. 117–126.
- [29] A. Blattmann et al., "Align your latents: High-resolution video synthesis with latent diffusion models," in *Proc. IEEE/CVF CVPR*, 2023, pp. 22563–22575.
- [30] J. Wolleb et al., "Diffusion models for implicit image segmentation ensembles," in *MIDL*, 2022, pp. 1336–1348.
- [31] T. Amit et al., "Segdiff: Image segmentation with diffusion probabilistic models," *arXiv preprint arXiv:2112.00390*, 2021.
- [32] J. Wu et al., "Medsegdiff: Medical image segmentation with diffusion probabilistic model," in *MIDL*, 2024, pp. 1623–1639.
- [33] J. Wu et al., "MedSegDiff-V2: Diffusion-Based Medical Image Segmentation with Transformer," in *Proc. AAAI Conf. Artif. Intell.*, vol. 38, no. 6, pp. 6030–6038, 2024.
- [34] H. Vu Quoc et al., "LSegDiff: A Latent Diffusion Model for Medical Image Segmentation," in *SOICT*, 2023, pp. 456–462.
- [35] F. A. Zaman et al., "Latent Diffusion for Medical Image Segmentation: End-to-End Learning for Fast Sampling and Accuracy," *arXiv preprint arXiv:2407.12952*, 2024.
- [36] M. Salsi et al., "Guided latent diffusion for universal medical image segmentation," in *Int. Conf. AI-Generated Content (AIGC)*, 2025, pp. 48–55.
- [37] Y. Lin, M. Xu, and S. Shit, "ProGiDiff: Prompt-Guided Diffusion-Based Medical Image Segmentation," *arXiv preprint arXiv:2601.16060*, 2026.
- [38] V. P. Nguyen et al., "Aleatoric Uncertainty Medical Image Segmentation Estimation via Flow Matching," in *Int. Workshop Uncertainty Safe Util. ML Med. Imaging*, 2025, pp. 134–144.
- [39] N. Codella et al., "Skin lesion analysis toward melanoma detection 2018," *arXiv preprint arXiv:1902.03368*, 2019.
- [40] D. Jha et al., "Kvasir-seg: A segmented polyp dataset," in *MMM*, 2020, pp. 451–462.
- [41] S. G. Armato III et al., "The lung image database consortium (LIDC) and image database resource initiative (IDRI)," *Med. Phys.*, vol. 38, no. 2, pp. 915–931, 2011.
- [42] I. Loshchilov, "Decoupled weight decay regularization," *arXiv preprint arXiv:1711.05101*, 2017.
- [43] L. Liu, Y. Ren, Z. Lin, and Z. Zhao, "Pseudo numerical methods for diffusion models on manifolds," *arXiv preprint arXiv:2202.09778*, 2022.
- [44] Z. Wang et al., "Image quality assessment: from error visibility to structural similarity," *IEEE Trans. Image Process.*, vol. 13, no. 4, pp. 600–612, 2004.
- [45] Q. Huynh-Thu and M. Ghanbari, "Scope of validity of PSNR in image/video quality assessment," *Electron. Lett.*, vol. 44, no. 13, pp. 800–801, 2008.